

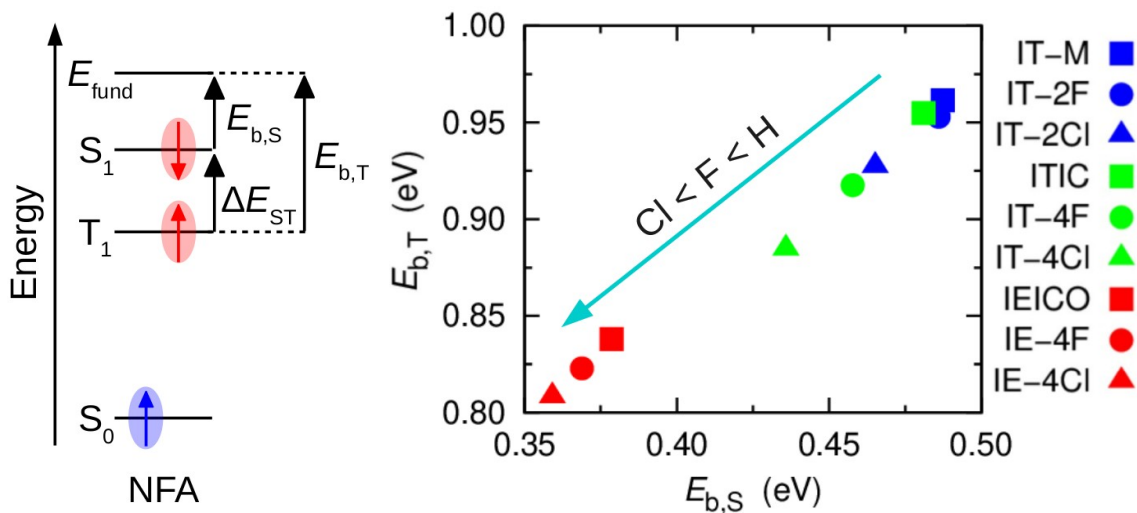
The Binding Energy of Triplet Excitons in Non-Fullerene Acceptors: The Effects of Fluorination and Chlorination

J. P. A. Souza,^a L. Benatto,^a G. Candioto,^b L. S. Roman^a and M. Koehler^a

^aDepartment of Physics, Federal University of Paraná, 81531-980, Curitiba-PR, Brazil

^bInstitute of Chemistry, Federal University of Rio de Janeiro, 21941-909, Rio de Janeiro-RJ, Brazil

Corresponding authors: joaojp@fisica.ufpr.br, koehler@fisica.ufpr.br



TOC Graph

Abstract

One strategy to improve the photovoltaic properties of non-fullerene acceptors (NFAs) is the rational fluorination or chlorination of those molecules. Although this modification improves important acceptor properties, little is known about the effects on the triplet states. Here, we combine the polarizable continuum model with optimally tuned range-separated hybrid functional to investigate this issue. We find that fluorination or chlorination of NFAs decreases the degree of HOMO-LUMO overlap along these molecules. Consequently, the energy gap between T_1 and S_1 states, $\Delta E_{ST}=E_{S_1}-E_{T_1}$, also decreases. This effect simultaneously enhances the generation of triplet excitons and reduce the binding energy of the triplet excitons ($E_{b,T}$) which favor their dissociation into free charges. Interestingly, although Cl has a lower electronegativity than F, the chlorination is more effective to reduce ΔE_{ST} . Since chlorination of NFAs is easier than fluorination, Cl substitution can be a useful approach to enhance solar energy harvesting using triplet excitons.

Over the years, the increased performance of organic solar cells (OSCs) has been directly linked to the development of more efficient organic semiconductor materials.^{1,2} Generally, two types of solution-processed organic semiconductors are employed in the active layer of OSCs: (i) electron donor polymer (D) and (ii) electron acceptor molecule (A). The combination of these two materials forms a D/A heterojunction.^{3,4} Currently, the performance of laboratory-scale OSCs are more than 18%⁵⁻⁷ which raises the potential for energy production using low cost devices processed by solution printing or coating techniques.^{8,9} In addition, the semi-transparency and flexibility characteristics of OSCs enable its application in an innovative way in comparison with inorganic solar cells.¹⁰

However, photoexcitation of organic semiconductors generates excitons that are coulombically bound electron-hole pairs.¹¹ The excitons formed in D or A can diffuse up to the D/A interface where they are more easily dissociated, thus generating free charges.¹²⁻¹⁴ The free charges are then transported to their respective electrodes, producing the device photocurrent response.¹⁵

In recent years, more efficient OSCs have been produced with non-fullerene acceptors (NFAs).¹⁶ Compared with traditional fullerene acceptors (FAs), NFAs have enhanced light absorption and tunable energy levels of the frontier molecular orbitals.^{17,18} In addition, NFAs have lower exciton binding energy of the singlet state,¹⁹ allowing the generation of free charges with lower driving force (energy difference between the local excited state and the charge transfer state).²⁰ A lower driving force is important to increase the device's open circuit voltage.²¹⁻²³ There are also reports of OSCs based on NFAs that showed very interesting characteristics such as ultrafast charge transfer,^{24,25} low charge trapping²⁶ and high morphological stability.²⁷ Despite these interesting characteristics of NFAs, further improvements have been sought.²⁸ Among them we can highlight the use of the two types of excited states, *i.e.*, singlets (S_1, \dots, S_n) and triplets (T_1, \dots, T_n), in the photovoltaic process.^{29,30}

Direct photon absorption in NFAs generates singlets excitons. Yet triplet excitons can be generated by intersystem crossing (ISC) and singlet fission.³¹ Triplet excitons are interesting because they have longer lifetimes than singlet excitons due to the forbidden nature of their recombination.³² In principle, this property can lead to longer diffusion lengths, which would tend to decrease the morphological constrains

associated to the sizes of the donors (acceptors) domains in bulk heterojunctions.^{33,34} On the other hand, triplet excitons have a higher binding energy compared to singlet excitons due to the attractive exchange interaction of the same spin orientation. This property makes them more difficult to dissociate. Importantly, when the energy gap between T_1 and S_1 decreases, $\Delta E_{ST}=E_{S1}-E_{T1}$, the exciton binding energy of the triplet exciton ($E_{b,T}$) approaches the binding energy of the singlet exciton ($E_{b,S}$) which would help the dissociation of the triplet excitons. In addition, the reduction of ΔE_{ST} enhances the intersystem crossing (ISC) from S_1 to T_1 which favors the generation of T_1 excitons.³⁵ Some of those characteristics of triplet and singlet excitons were experimentally observed in oligoacenes by Hummer *et al.*³⁶ and theoretically reproduced with good precision by Hu *et al.*³⁷ In the latter study, the calculations were performed combining the polarizable continuum model (PCM) and optimally tuned range-separated (RS) hybrid functional. From a theoretical point of view, the great importance of considering solid-state polarization effects for the stabilization of singlet and triplet energies was stressed by Chen and coauthors.³⁸

The decrease in ΔE_{ST} is essential to improve the use of triple excitons in the photovoltaic process. Considering a simple two-electron two-state model, it is possible to obtain the relation $\Delta E_{ST} = 2K_{HL}$,³⁸ where K_{HL} is the electron exchange energy between electron 1 in the HOMO (highest occupied molecular orbital) and electron 2 in the LUMO (lowest unoccupied molecular orbital). K_{HL} depends on the degree of HOMO–LUMO overlap (Θ_{H-L}) and can be reduced with the minimization of Θ_{H-L} . Organic molecules with high twisted D–A structure can effectively separate the HOMO and LUMO ($\Theta_{H-L} \approx 0$) reaching a very small values of ΔE_{ST} .³⁹ The two main problems of a twisted molecular structure for OSCs applications is the weak oscillator strength (f) of the $S_0 \rightarrow S_1$ transition which limits the light absorption and the poor charge carriers mobility over the molecules.³⁵ Both problems are associated to the reduction in the average conjugated length induced by the twisted structure. In a recent study Qin and coauthors³⁵ demonstrated that A-D-A-D-A-type NFAs, analogues of Y6,⁴⁰ with low twisted conformation (two halves of the molecules share a dihedral angle of approximately 17°) have promising ΔE_{ST} of approximately 0.35 eV and long lifetime excitons of the order of 50 ns in blend films. In their calculation of ΔE_{ST} , E_{S1} was considered equal to the optical band gap extracted from external quantum efficiency

spectra and E_{T1} extracted from the onset of the emission band of the film at low temperature. The effective generation and split of triplet excitons has been reported, contributing to the device photocurrent. Interestingly, the two NFAs considered by Qin presented chlorine and fluorine end-groups.

The promising perspectives for the use of triplet excitons in the photovoltaic process of OSCs^{34,41} have motivated us to study more deeply the influence of fluorine and chlorine substitutions on the properties of triplet states generated in NFAs. The fluorination and chlorination processes of organic materials have been widely used in recent years.⁴² Both procedures cause similar changes in the morphological and optoelectronic properties of NFAs. A significant improvement in the crystallinity of the formed films was reported, which increases the electronic coupling between molecular orbitals of adjacent molecules and consequently the mobility of electrons.⁴³ Furthermore, it is reported a shift of the frontier energy levels and a broadening of the absorption spectrum specially with the chlorination.⁴⁴ Because the synthesis of chlorinated acceptors is simpler than the synthesis of fluorinated ones, the use of Cl substitutions might be more convenient to reduce large scale production costs for NFA-based OSCs.^{45,46}

Here, we will simulate nine NFAs that have a fused acceptor-donor-acceptor linear structure (A-D-A). They can be separated into three groups of three molecules, as shown in Figure 1. Each group contains an unsubstituted molecule, a fluorinated molecule and a chlorinated molecule. The first group consists of the IT-M,⁴⁷ IT-2F⁴⁸ and IT-2Cl,⁴⁴ where the F or Cl atoms replace the methyl attached to the IT-M acceptor units. The second group consists of the ITIC,⁴⁹ IT-4F⁵⁰ and IT-4Cl,⁴⁴ where the F or Cl atoms replace two hydrogens of the ITIC acceptor units. Finally the third group consists of the IEICO,⁵¹ IE-4F⁵² and IE-4Cl,⁵³ where the F or Cl atoms replace two hydrogens of the IEICO acceptor units.

Note that the three groups of NFAs have four side chains linked to the central donor unity. However, group III molecules have two differences from group I and II molecules. The first is a smaller number of aromatic fused rings in the central donor unit, specifically two less fused rings. Note that the fused thiophene present in the central donor unit of the groups I and II molecules make a single bound with this unit in the group III molecules. This modification increases the molecular length of group III

molecules. The second difference of group III molecules are two additional side chains linked to thiophenes.

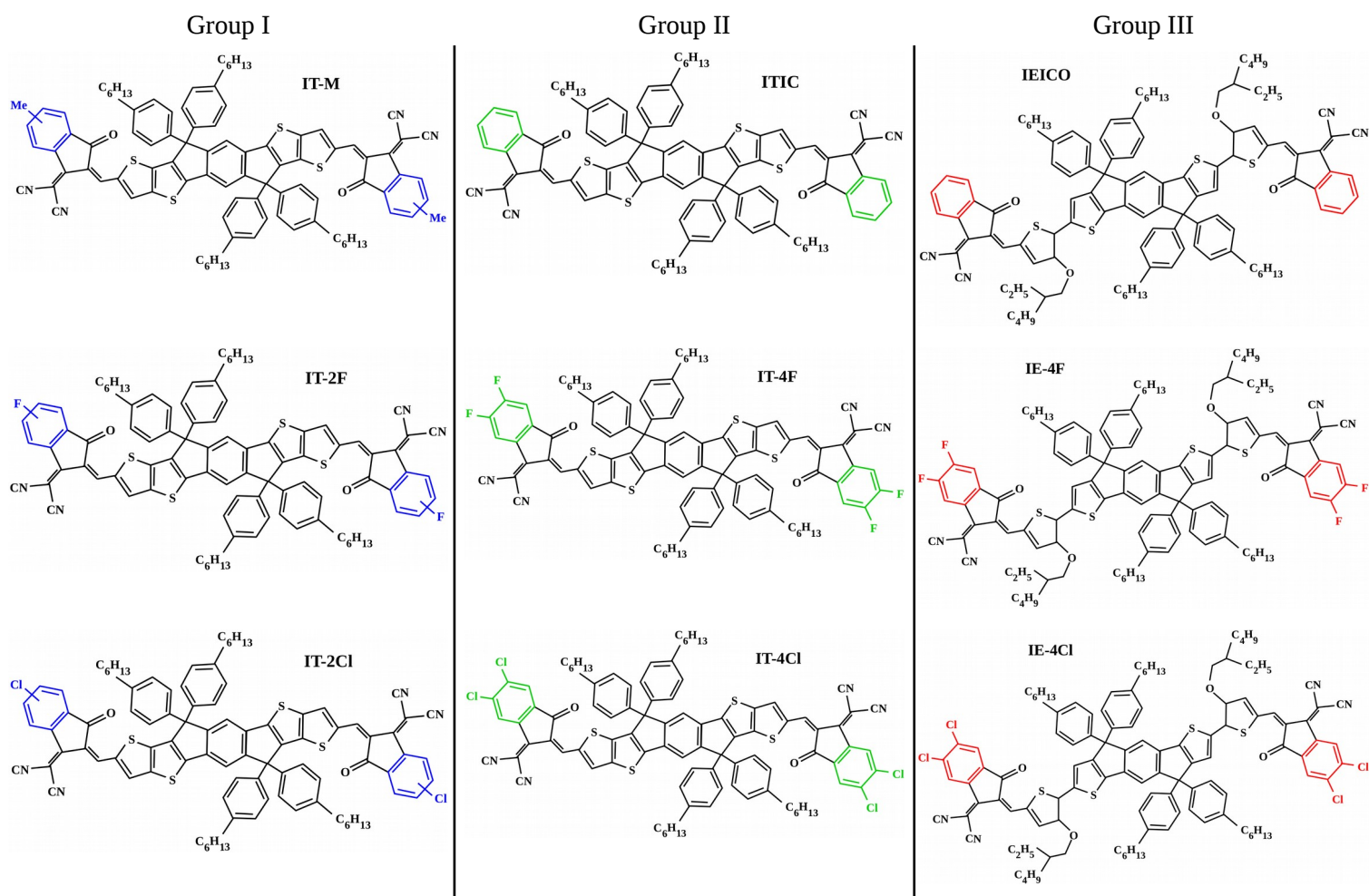


Figure 1 – Chemical structure of the three groups of NFAs.

We have applied density functional theory (DFT) and time-dependent DFT (TDDFT) calculations to study the key properties of acceptor molecules. All DFT/TDDFT calculations were performed using the Gaussian 16 package.⁵⁴

The first step of our calculations is to optimize the ground state geometry of isolated materials by DFT with the Becke three-parameter Lee-Yang-Parr (B3LYP)⁵⁵ hybrid functional and 6-31G(d,p) basis set. To obtain a good description of the molecular energies, the electronic properties of the optimized molecules were calculated *via* DFT/TDDFT using ω B97XD⁵⁶ the range-separated hybrid functional with empirical dispersion corrections along 6-31G(d,p) basis set.⁵⁷ Besides that, the

range-separation parameter (ω) of the functional ω B97XD was optimized following the gap adjustment procedure. In this procedure, ω is adjusted to minimize $J(\omega)$:^{58,59}

$$J(\omega) = |E_{HOMO}(\omega) - IP(\omega)| + |E_{LUMO}(\omega) - EA(\omega)| \quad (1)$$

where $E_{HOMO}(\omega)$ and $E_{LUMO}(\omega)$ are the energies of the HOMO and LUMO while $IP(\omega)$ and $EA(\omega)$ are the vertical first ionization potential and electron affinity of the material, respectively. With the total energies of the cationic (E_+), anionic (E_-), and neutral (E_0) states it is possible to calculate $IP = E_+ - E_0$ and $EA = E_0 - E_-$.⁶⁰ This procedure was performed using the polarizable continuum model⁶¹ (PCM) to simulate the molecule in a dielectric medium. It was found that these methods was able to calculate molecular energies that are in better agreement with experimental values.^{37,62,63} The dielectric constants of each molecule for the PCM calculation were obtained from ref⁶⁴. We also calculated the atomic charges *via* the electrostatic potential (ESP) method⁶⁵⁻⁶⁷ to obtain the magnitude of the internal charge transfer (ICT) between the acceptor chemical units and the donor chemical unit of the molecules. The degree of HOMO-LUMO overlap were obtained by the Multiwfn program.⁶⁸

The exciton binding energy can be calculated by subtracting the fundamental energy gap ($E_{fund} = IP - EA$) from the optical gap.⁶⁰ The optical gap can be obtained from TDDFT calculations and corresponds to E_{S1} and E_{T1} for singlet and triplet. Therefore, the binding energy of singlet ($E_{b,S}$) and triplet ($E_{b,T}$) exciton is defined as:

$$E_{b,S} = E_{fund} - E_{S1} \quad (2)$$

and

$$E_{b,T} = E_{fund} - E_{T1}. \quad (3)$$

In the sequence we will detail the results obtained using the methods described above. We will pay special attention to the variations in the triplet exciton binding energy with the fluorination and chlorination of the NFAs.

The comparison of the theoretical results of IP , EA and E_{S1} with experimental data obtained by Yang and coauthors⁶⁹ can be seen in Table 1 and Figure 2. The three groups of molecules show a similar pattern with respect to the variation of the molecular

energies. IP and EA increase with the fluorination or chlorination of the molecules and the opposite occurs for E_{S1} . Notice that the variations are greater with the chlorination. We anticipate that this same pattern will be observed below for other electronic properties, *i.e.*, the improvements on key molecular features are higher for chlorination than for fluorination. The correlation coefficient (R_{sq}) calculated through the linear adjustment of theoretical and experimental values of IP, EA and E_{S1} resulted in approximately 0.975, 0.933 and 0.943, respectively. The quality of the linear regression to reproduce the data increases as R_{sq} approaches 1. Thus, there is a reasonable correlation between the theoretical and experimental values of IP, with the theoretical values being on average 0.34 eV lower. For EA the correlation is smaller, where the theoretical values are on average 0.79 eV lower. It is expected a greater deviation from the experimental data for the values of EA since the calculation of this parameter is more sensitive to delocalization error associated with the exchange-correlation functional.⁷⁰ Here we point out that comparisons between energies estimated using vertical electronic transitions with energies measured by adiabatic processes (like the CV technique) must always be interpreted with caution. Considering E_{S1} , there is a very good correlation between theory and experiment, being the mean deviation of 0.03 eV.

Table 1 - Optimal Range-Separation Parameter ω (in Bohr⁻¹). Theoretical results – in solid with PCM – compared to measurements of IP, EA and E_{S1} energies (in eV).

| Molecules | ω | IP | | EA | | E_{S1} | |
|-----------|----------|-------|-------------------|-------|-------------------|----------|-------------------|
| | | Theo. | Exp. ^a | Theo. | Exp. ^a | Theo. | Exp. ^a |
| IT-M | 0.0030 | 5.35 | 5.64 | 3.10 | 3.90 | 1.76 | 1.77 |
| I IT-2F | 0.0030 | 5.42 | 5.69 | 3.20 | 3.99 | 1.72 | 1.73 |
| IT-2Cl | 0.0023 | 5.43 | 5.70 | 3.24 | 4.02 | 1.68 | 1.73 |
| ITIC | 0.0022 | 5.38 | 5.66 | 3.14 | 3.93 | 1.75 | 1.76 |
| II IT-4F | 0.0010 | 5.43 | 5.72 | 3.24 | 4.03 | 1.70 | 1.73 |
| IT-4Cl | 0.0011 | 5.46 | 5.73 | 3.32 | 4.08 | 1.64 | 1.70 |
| IEICO | 0.0006 | 4.95 | 5.38 | 3.12 | 3.90 | 1.53 | 1.45 |
| III IE-4F | 0.0013 | 5.00 | 5.46 | 3.20 | 4.04 | 1.43 | 1.42 |
| IE-4Cl | 0.0001 | 5.03 | 5.49 | 3.28 | 4.08 | 1.40 | 1.39 |

^a Experimental results of ref⁶⁹ in which IP and EA was estimated from electrochemical measurements with cyclic voltammetry (CV) and E_{S1} was estimated from the first maximum absorption wavelength (λ_{max}) in thin film.

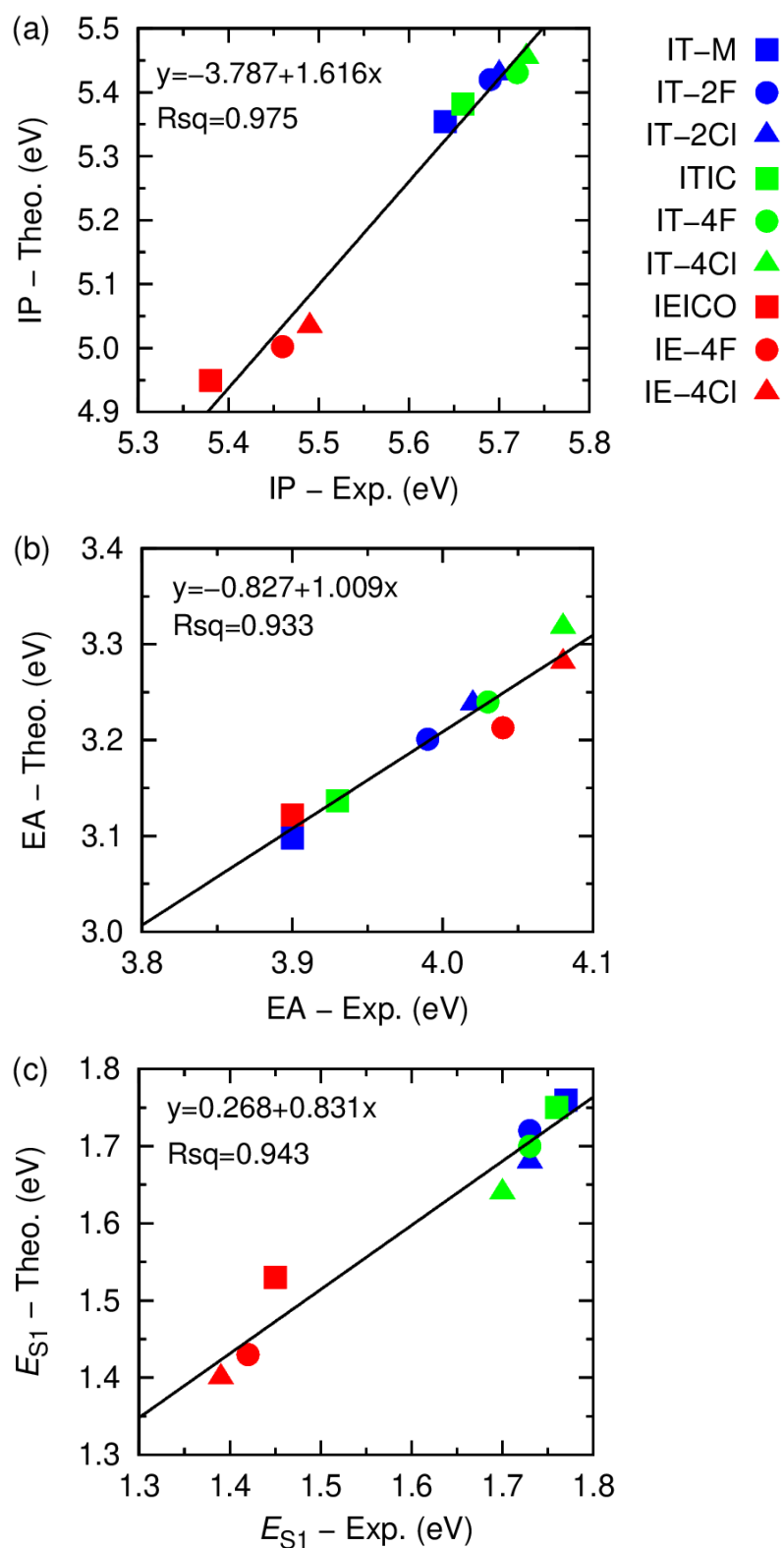


Figure 2 - Correlation between theoretical and experimental results of IP, EA and E_{S1} for the three groups of NEAs. The linear equation and the the squared correlation coefficient (R_{sq}) are displayed in detail.

Although NFAs have a low electric dipole moment due to their symmetry and planarity, when the acceptor units of the molecules are modified by F or Cl substitution, this molecular property undergoes variations induced by the higher electronegativity of those atoms. Indeed, Figure 3a shows that the unsubstituted molecules of the three groups (IT-M, ITIC and IEICO) have an electrical dipole moment very close to zero. With the addition of F atoms in the chemical structure of the molecules the electric dipole moment undergoes a slight increase. For the molecules with Cl the increase is even greater. This effect is related to the strong electronegativity of the F and Cl atoms, making the acceptor groups of the molecules more negative.^{44,71} Consequently, the central donor unit becomes more positive. This change in the distribution of the molecular charge can be estimated by obtaining the magnitude of the ICT between the acceptor and donor moieties. The magnitude of ICT for each molecule are presented in Fig. 3b. There is a certain correlation between ICT and the intensity of electric dipole moment of the molecules so that the NFAs with higher ICT within each group tend to have a stronger dipole moment. Note that the molecules of group III have the highest values of ICT. For example, IE-4Cl had ICT = 0.61 electron compared to ICT = 0.51 electron for IT-2Cl (that belongs to group I).

It is known that the electronegativity of fluorine is stronger than chlorine (Pauline electronegativity⁷² for Cl: 3.16; for F: 3.98). Yet Figure 3 demonstrates that the acceptor molecules with chlorine presented the highest values of dipole moment and ICT. This result can be related to the significantly longer C–Cl bond (~ 1.74 Å) than C–F bond (~ 1.34 Å) that helps to separate the electron from the central core (D unit). These changes in the molecular structure and charge distribution reflect on the electronic energy levels and exciton binding energy. A deeper discussion on the subtle differences on the effects induced by the F or Cl substitution will be developed below.

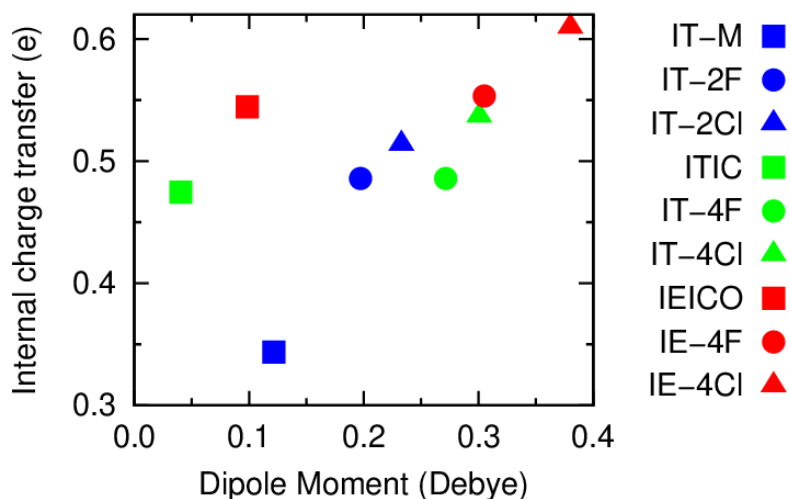


Figure 3 – Dipole moment and internal charge transfer for the three groups of NFAs.

Figure 4 shows the calculated vertical excitation energies and oscillator strength (f) of the $S_0 \rightarrow S_1$ transition. The magnitudes of f indicates a high probability of photon absorption for energies corresponding to the $S_0 \rightarrow S_1$ transition. On the other hand, as expected, $f = 0$ for the $S_0 \rightarrow T_n$ transition so that the direct photoexcitation of triplet states is extremely improbable. Consequently, the triplet generation depends on an efficient intersystem crossing process that can be improved by the reduction of ΔE_{ST} .³⁵ Another important result from Fig. 4 is that the energies of the excited states S_1 , T_1 , T_2 and T_3 decreased with the F or Cl substitutions.

From Figure 4 it is possible to obtain the energy gap between T_1 and S_1 states, ΔE_{ST} (see inset). The fluorination dropped ΔE_{ST} by 0.01 eV on average. Using DFT calculation, Han and coauthors³⁰ recently found the same decrease of ΔE_{ST} with the fluorination of ITIC. Here we obtained that chlorination decreases ΔE_{ST} by 0.02 eV on average, double of the reduction produced by fluorination.

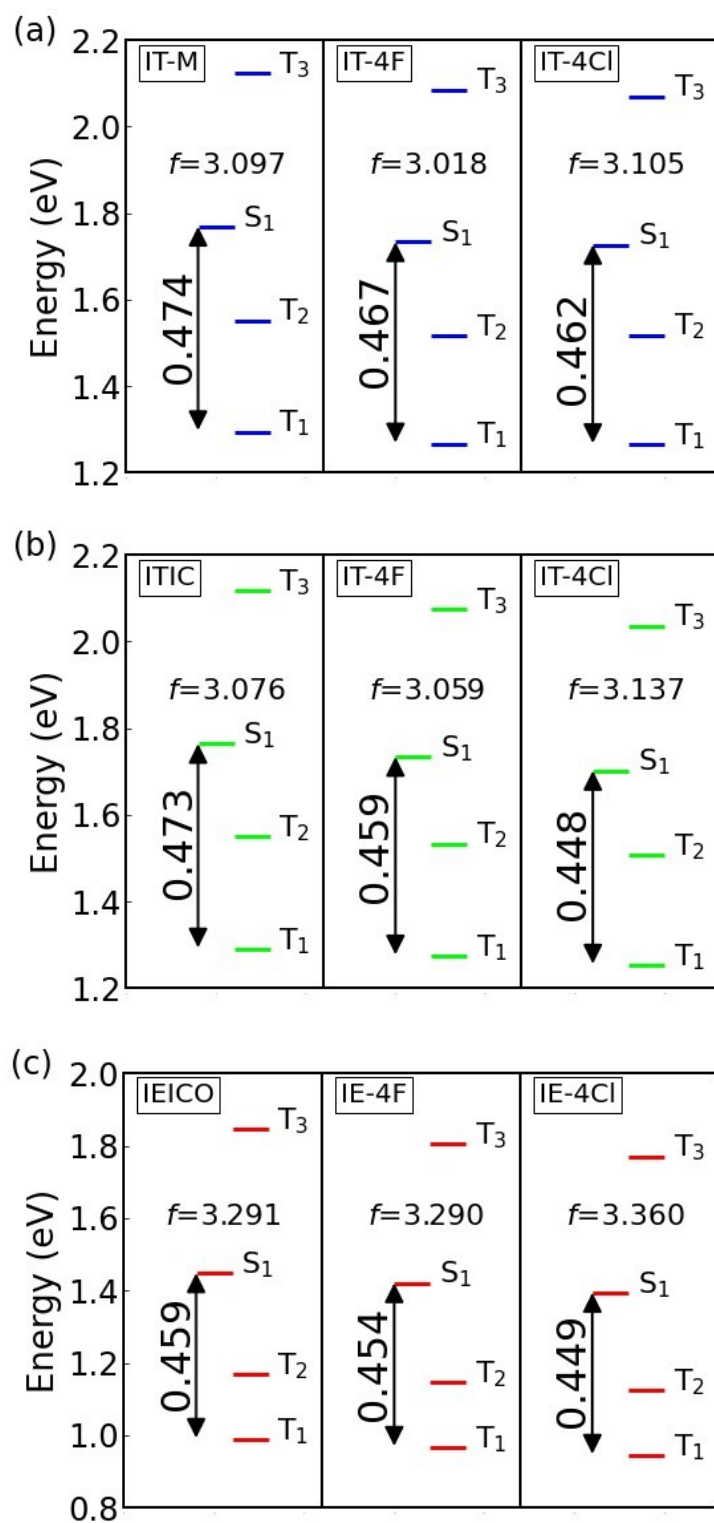


Figure 4 - Vertical excitation energies and oscillator strength (f) of the $S_0 \rightarrow S_1$ transition for the three groups of NFAs. Inset: double arrows represent the energy gap between T_1 and S_1 states ($\Delta E_{ST} = E_{S_1} - E_{T_1}$).

The frontier molecular orbitals HOMO and LUMO of the three groups of NFAs

was presented in Figure 5 together with the degree of HOMO-LUMO overlap, $\Theta_{\text{H-L}}$, and the weights of the HOMO \rightarrow LUMO transition in the S1 and T1 excitations. Note that the HOMO is localized mainly in the central donor unit of the molecules whereas the LUMO is localized mainly in the end-group. $\Theta_{\text{H-L}}$ decreases by approximately 1% with fluorination. The molecules with Cl (apart from group I molecules) have even smaller $\Theta_{\text{H-L}}$ compared to molecules with F. From Figs 4 and 5, one can see that there is a relationship between ΔE_{ST} and $\Theta_{\text{H-L}}$ where smaller values of $\Theta_{\text{H-L}}$ tend to reduce ΔE_{ST} . This effect is a result of the lower degree of HOMO-LUMO overlap which increases the average distance between the photo-excited electron and hole pair. Since exchange interactions have a short range, this effect approaches the triplet and singlet energies. Furthermore, the IE-4Cl acceptor has the lowest values of $\Theta_{\text{H-L}} = 62.8\%$. The extended central unity of IEICO based-molecules helps to decrease the degree of HOMO-LUMO overlap. From our calculations, the molecular length, l , of the molecules are presented in Figure 5.

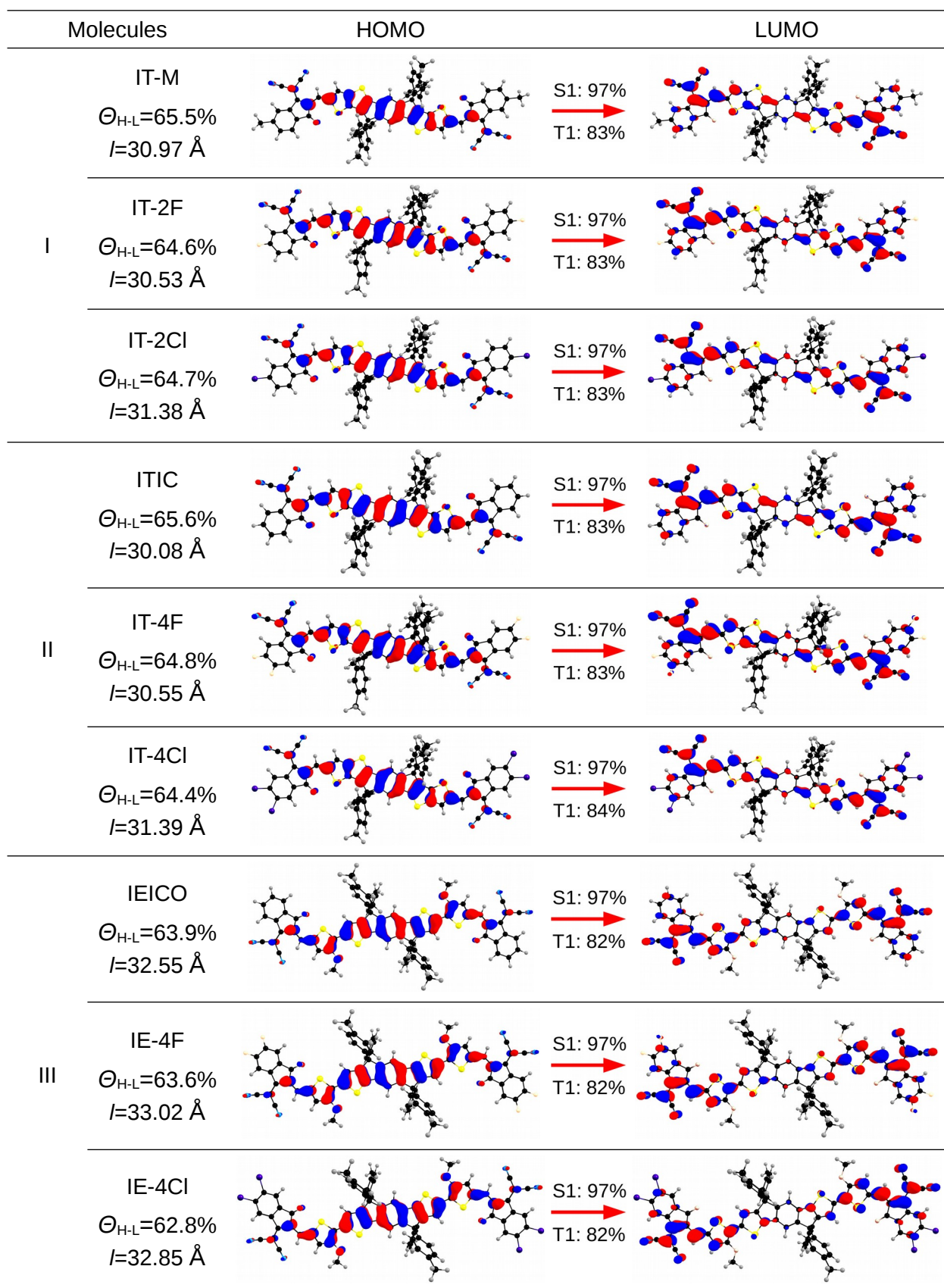


Figure 5 – Frontier molecular orbitals for the three groups of NFAs (isovalues 0.02), degree of HOMO-

LUMO overlap, Θ_{H-L} , and molecular length, l . The weights of the HOMO \rightarrow LUMO transition in the S1 and T1 excitations are provided.

Associated to the ΔE_{ST} reduction, there is consequent decrease of $E_{b,T}$ (Fig. 6). The average drop of $E_{b,T}$ upon fluorination (chlorination) in Fig. 6 was 0.02 eV (0.04 eV). This average decrease is higher compared to the reduction observed for the binding energy of singlet excitons ($E_{b,S}$), around 0.01 eV (0.03 eV) upon fluorination (chlorination). Among all groups, lower values of $E_{b,T}$ and $E_{b,S}$ were calculated for group III NFAs which can be attributed to the longer molecular length of the IEICO derivatives.⁷³ Within group III, however, IE-4Cl have the lowest values of $E_{b,T}$ and $E_{b,S}$ (0.81 eV and 0.36 eV, respectively). Note that in general $E_{b,T}$ is approximately twice as large as $E_{b,S}$. Although the $E_{b,T}$ magnitudes are high (between 0.96-0.8 eV), these values are similar to the $E_{b,S}$ values of FAs.^{19,20} Therefore, it is possible to find a suitable combination of D/NFAs blends with a driving force high enough to dissociate triplet excitons generated in the NFAs. Yet an even larger reduction of $E_{b,T}$ is desirable in order to use these excitons also in low driving force systems. In a broader context regarding interfacial energy levels in D/NFAs blends of organic solar cells, it is very desirable that E_{T1} becomes higher than the energy of charge transfer (CT) state or at least close to E_{CT} .⁷⁴ A higher value of E_{T1} tends to decrease the transfer rate from CT to T_1 and increases the transfer rate from T_1 to CT. Importantly, this effect would mitigate the non-radiative recombination pathway from T_1 to S_0 , contributing to decrease the voltage losses.⁷⁵

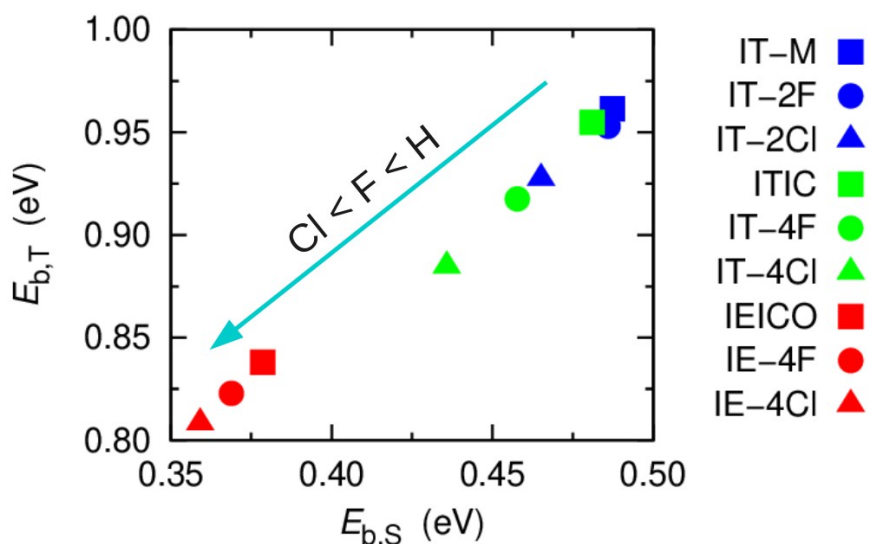


Figure 6 – Binding energy of triplet exciton and singlet exciton for the three groups of NFAs. The arrow indicates the behavior of energies due to replacement of H atoms by F or Cl.

Even though F is more electronegative than Cl, all the results showed above indicates that the chlorine substitution is more effective than fluorine substitution to decrease Θ_{H-L} and, consequently, to lower ΔE_{ST} and $E_{b,T}$. This tendency appears to be counterintuitive and deserves a further analysis. As it was already observed for other organic semiconductors with Cl substitutions, the addition of chlorine atoms tends to significantly stabilize the LUMO but it almost does not change the energy of the HOMO (compared to the unsubstituted or F substitute molecular counterparts⁷²). Indeed, this effect can be verified in the results of Table 1 when comparing the EA and IP variations. In addition, Figure 5 reveals differences in the LUMO distribution among Cl and F substitute molecules. There is increased density of LUMO states in the vicinities of the chlorine atoms relative to the density of those states around the F atoms. This result indicates that there will be a higher electronic delocalization once an electron is promoted to unoccupied states of the LUMO for the molecules with Cl substitution. As suggested in Ref.⁷², this effect is related to the fact that Cl atoms has empty 3d orbitals to harbor any delocalization of the pi-electrons. In contrast, the next unoccupied atomic orbital of F atoms is the 3s level which is more localized and higher in energy. Moreover, fluorine atoms have a smaller radius that results in considerable electrostatic repulsion in the case of pi-electron delocalization in its vicinities. Hence higher degree of electronic delocalization of the excited electron around the Cl atoms might be the

final reason behind the improved properties of the chlorinated NFAs.

At this point it is important to mention that we are using polarizable continuum model to describe the solid-state effects. Since this method is an effective medium approximation, an improvement of the calculations would be obtained by considering intermolecular interaction in different conformations. This approach would reveal the influence of packing in the molecular energies.^{76,77} In general, the molecular packing tends to reduce the energies of electronic transitions.^{19,31} It was verified by Han *et al.* that this effect is more pronounced for E_{S1} than E_{T1} , which further reduces the magnitude of ΔE_{ST} in approximately 0.1 eV.³⁰ Additionally, it is also important to investigate the rate of intersystem crossing from singlet to triplet state. This parameter depends on the ΔE_{ST} , the spin-orbit coupling, and the reorganization energy.^{78,79}

Finally, in addition to spin-orbit effects, triplet excitons can also be generated from singlet fission through singlet–singlet exciton annihilation (SSA). This effect is especially relevant at high excitation fluences.^{33,80,81} Using transient absorption spectroscopy Natsuda *et al.*⁸², had recently suggested that this mechanism of triplet formation is dominant in Y6, another important non-fullerene acceptor. Interesting, they attribute the ultrafast triplet exciton formation to higher excited singlet states (S_n states) that satisfies the energetic requirement for singlet fission, $E_S > 2E_T$. It is possible that these mechanisms may also occur with the NFAs studied here and should be investigated in a future work.

In conclusion, we studied the singlet-triplet gap and the binding energy of triplet excitons for nine typical NFAs. Those properties were calculated using the polarizable continuum model with optimally tuned range-separated hybrid functional. We find that the rational fluorination and chlorination of NFAs can be an effective way to improve the internal charge transfer and decrease the degree of HOMO-LUMO overlap of these molecules. These changes favor the generation of triplet excitons and reduce the binding energy of the singlet and triplet excited states specially for those acceptors with Cl substitutions. Among the three groups of NFAs considered here, IEICO derivatives have the lower exciton binding energies due to the longer conjugation length of those molecules. The molecules with the lowest values of ΔE_{ST} are IT-4Cl (0.448 eV) and IE-4Cl (0.449 eV). Although the magnitude of $E_{b,T}$ (between 0.8 and 0.96 eV) is approximately twice as large than $E_{b,S}$ for NFAs, the magnitudes are similar to $E_{b,S}$ of

traditional fullerene acceptors. To our knowledge, this is the first study indicating that the chlorination can be a promising strategy to decrease the binding energy of triplet exciton in commonly used NFAs. In addition, considering the active layer of OSCs formed by D/NFAs bulk heterojunctions, higher values of E_{T1} induced by Cl substitutions of the acceptor might decrease non-radiative recombination losses produced by the CT deactivation via T_1 states.

The utilization of triplet excitons to enhance charge generation is one promising step to further improve performance of OSCs. In this context, our findings indicate that rational chlorination of the acceptors can be an additional advantage towards more efficient OSCs. This observation is significant since chlorinated precursors are more easily available and are cheaper than fluorinated ones.⁸³

Conflicts of interest

The authors declare no conflicts of interest.

Acknowledgments

This work has been partially supported by the Companhia Paranaense de Energia – COPEL research and technological development program, through the PD 2866-0470/2017 project, regulated by ANEEL. This study was financed in part by the Coordenação de Aperfeiçoamento de Pessoal de Nível Superior-Brasil (CAPES)-Finance Code 001. Research developed with the assistance of CENAPAD-SP (Centro Nacional de Processamento de Alto Desempenho em São Paulo), project UNICAMP/FINEP – MCT and Sistema Nacional de Processamento de Alto Desempenho (SINAPAD/SDUMONT). Special thanks go to CAPES-PrInt-UFRJ, CNPq (grant 381113/2021-3) and to LCNano/SisNANO 2.0 (grant 442591/2019-5) for financial support. G. Candioto gratefully acknowledges FAPERJ Process E-26/200.008/2020 for financial support and Núcleo Avançado de Computação de Alto Desempenho (NACAD/COPPE/UFRJ).

References

- (1) Zhou, H.; Yang, L.; You, W. Rational Design of High Performance Conjugated

- Polymers for Organic Solar Cells. *Macromolecules* **2012**, *45*, 607–632.
- (2) Yao, C.; Yang, Y.; Li, L.; Bo, M.; Zhang, J.; Peng, C.; Huang, Z.; Wang, J. Elucidating the Key Role of the Cyano (-CN) Group to Construct Environmentally Friendly Fused-Ring Electron Acceptors. *J. Phys. Chem. C* **2020**, *124* (42), 23059–23068.
 - (3) Wadsworth, A.; Moser, M.; Marks, A.; Little, M. S.; Gasparini, N.; Brabec, C. J.; Baran, D.; McCulloch, I. Critical Review of the Molecular Design Progress in Non-Fullerene Electron Acceptors towards Commercially Viable Organic Solar Cells. *Chem. Soc. Rev.* **2019**, *48* (6), 1596–1625.
 - (4) Han, G.; Yi, Y. Rationalizing Small-Molecule Donor Design toward High-Performance Organic Solar Cells: Perspective from Molecular Architectures. *Adv. Theory Simulations* **2018**, *1* (11), 1800091.
 - (5) Liu, Q.; Jiang, Y.; Jin, K.; Qin, J.; Xu, J.; Li, W.; Xiong, J.; Liu, J.; Xiao, Z.; Sun, K.; et al. 18% Efficiency Organic Solar Cells. *Sci. Bull.* **2020**, *65* (4), 272–275.
 - (6) Zhang, M.; Zhu, L.; Zhou, G.; Hao, T.; Qiu, C.; Zhao, Z.; Hu, Q.; Larson, B. W.; Zhu, H.; Ma, Z.; et al. Single-Layered Organic Photovoltaics with Double Cascading Charge Transport Pathways: 18% Efficiencies. *Nat. Commun.* **2021**, *12* (1), 1–10.
 - (7) Bi, P.; Zhang, S.; Beijing, T.; Chen, Z. Reduced Non-Radiative Charge Recombination Enables Organic Photovoltaic Cell Approaching 19% Efficiency. *Joule* **2021**, *5*, 1–12.
 - (8) Meng, X.; Zhang, L.; Xie, Y.; Hu, X.; Xing, Z.; Huang, Z.; Liu, C.; Tan, L.; Zhou, W.; Sun, Y.; et al. A General Approach for Lab-to-Manufacturing Translation on Flexible Organic Solar Cells. *Adv. Mater.* **2019**, *1903649*, 1903649.
 - (9) Cui, Y.; Wang, Y.; Bergqvist, J.; Yao, H.; Xu, Y.; Gao, B.; Yang, C.; Zhang, S.; Inganäs, O.; Gao, F.; et al. Wide-Gap Non-Fullerene Acceptor Enabling High-Performance Organic Photovoltaic Cells for Indoor Applications. *Nat. Energy* **2019**, *4* (9), 768–775.
 - (10) Dong, S.; Zhang, K.; Xie, B.; Xiao, J.; Yip, H. L.; Yan, H.; Huang, F.; Cao, Y. High-Performance Large-Area Organic Solar Cells Enabled by Sequential Bilayer Processing via Nonhalogenated Solvents. *Adv. Energy Mater.* **2019**, *9* (1), 1–7.
 - (11) Zhang, J.; Zhu, L.; Wei, Z. Toward Over 15% Power Conversion Efficiency for Organic Solar Cells: Current Status and Perspectives. *Small Methods* **2017**, *1* (12), 1700258.

- (12) Dimitrov, S. D.; Schroeder, B. C.; Nielsen, C. B.; Bronstein, H.; Fei, Z.; McCulloch, I.; Heeney, M.; Durrant, J. R. Singlet Exciton Lifetimes in Conjugated Polymer Films for Organic Solar Cells. *Polymers (Basel)*. **2016**, *8* (1), 14.
- (13) Sousa, L. E.; Coropceanu, V.; da Silva Filho, D. A.; Sini, G. On the Physical Origins of Charge Separation at Donor–Acceptor Interfaces in Organic Solar Cells: Energy Bending versus Energy Disorder. *Adv. Theory Simulations* **2020**, *3* (4), 1900230.
- (14) Firdaus, Y.; Corre, V. M. Le; Karuthedath, S.; Liu, W.; Markina, A.; Huang, W.; Chattopadhyay, S.; Nahid, M. M.; Nugraha, M. I.; Lin, Y.; et al. Long-Range Exciton Diffusion in Molecular Non-Fullerene Acceptors. *Nat. Commun.* **2020**, *11*, 1–10.
- (15) Proctor, C. M.; Kuik, M.; Nguyen, T.-Q. Charge Carrier Recombination in Organic Solar Cells. *Prog. Polym. Sci.* **2013**, *38* (12), 1941–1960.
- (16) Meredith, P.; Li, W.; Armin, A. Nonfullerene Acceptors: A Renaissance in Organic Photovoltaics? *Adv. Energy Mater.* **2020**, *10* (33), 2001788.
- (17) Liu, Z.; Zhang, X.; Li, P.; Gao, X. Recent Development of Efficient A-D-A Type Fused-Ring Electron Acceptors for Organic Solar. *Sol. Energy* **2018**, *174* (July), 171–188.
- (18) Chen, W.; Zhang, Q. Recent Progress in Non-Fullerene Small Molecule Acceptors in Organic Solar Cells (OSCs). *J. Mater. Chem. C* **2017**, *5* (6), 1275–1302.
- (19) Benatto, L.; Marchiori, C. F. N.; Araujo, C. M.; Koehler, M. Molecular Origin of Efficient Hole Transfer from Non-Fullerene Acceptors: Insights from First-Principles Calculations. *J. Mater. Chem. C* **2019**, *7* (39), 12180–12193.
- (20) Zhu, L.; Yi, Y.; Wei, Z. Exciton Binding Energies of Non-Fullerene Small Molecule Acceptors: Implication for Exciton Dissociation Driving Forces in Organic Solar Cells. *J. Phys. Chem. C* **2018**, *122* (39), 22309–22316.
- (21) Han, G.; Yi, Y. Origin of Photocurrent and Voltage Losses in Organic Solar Cells. *Adv. Theory Simulations* **2019**, *2* (8), 1900067.
- (22) Eisner, F. D.; Azzouzi, M.; Fei, Z.; Hou, X.; Anthopoulos, T. D.; Dennis, T. J. S.; Heeney, M.; Nelson, J. Hybridization of Local Exciton and Charge-Transfer States Reduces Nonradiative Voltage Losses in Organic Solar Cells. *J. Am. Chem. Soc.* **2019**, *141* (15), 6362–6374.
- (23) Han, G.; Yi, Y. Local Excitation/Charge-Transfer Hybridization Simultaneously Promotes Charge Generation and Reduces Nonradiative Voltage Loss in

- Nonfullerene Organic Solar Cells. *J. Phys. Chem. Lett.* **2019**, *10*, 2911–2918.
- (24) Zhong, Y.; Causa', M.; Moore, G. J.; Krauspe, P.; Xiao, B.; Günther, F.; Kublitski, J.; Shivhare, R.; Benduhn, J.; BarOr, E.; et al. Sub-Picosecond Charge-Transfer at near-Zero Driving Force in Polymer:Non-Fullerene Acceptor Blends and Bilayers. *Nat. Commun.* **2020**, *11* (1), 833.
- (25) Bolzonello, L.; Bernal-texca, F.; Gerling, L. G.; Ockova, J.; Collini, E.; Martorell, J.; Hulst, N. F. Van. Photocurrent-Detected 2D Electronic Spectroscopy Reveals Ultrafast Hole Transfer in Operating PM6/Y6 Organic Solar Cells. *J. Phys. Chem. Lett.* **2021**, *12*, 3983–3988.
- (26) Wu, J.; Lee, J.; Chin, Y.-C.; Yao, H.; Cha, H.; Luke, J.; Hou, J.; Kim, J.-S.; Durrant, J. R. Exceptionally Low Charge Trapping Enables Highly Efficient Organic Bulk Heterojunction Solar Cells. *Energy Environ. Sci.* **2020**, *13* (8), 2422–2430.
- (27) Holliday, S.; Ashraf, R. S.; Wadsworth, A.; Baran, D.; Yousaf, S. A.; Nielsen, C. B.; Tan, C. H.; Dimitrov, S. D.; Shang, Z.; Gasparini, N.; et al. High-Efficiency and Air-Stable P3HT-Based Polymer Solar Cells with a New Non-Fullerene Acceptor. *Nat. Commun.* **2016**, *7*, 1–11.
- (28) Wang, Y.; Lee, J.; Hou, X.; Labanti, C.; Yan, J.; Mazzolini, E.; Parhar, A.; Nelson, J.; Kim, J. S.; Li, Z. Recent Progress and Challenges toward Highly Stable Nonfullerene Acceptor-Based Organic Solar Cells. *Adv. Energy Mater.* **2021**, *11* (5), 1–41.
- (29) Zhao, F.; Wang, K.; Duan, J.; Zhu, X.; Lu, K.; Zhao, C.; Zhang, C.; Yu, H.; Hu, B. Spin-Dependent Electron–Hole Recombination and Dissociation in Nonfullerene Acceptor ITIC-Based Organic Photovoltaic Systems. *Sol. RRL* **2019**, *3* (7), 1–9.
- (30) Han, G.; Hu, T.; Yi, Y. Reducing the Singlet–Triplet Energy Gap by End-Group Π – π Stacking Toward High-Efficiency Organic Photovoltaics. *Adv. Mater.* **2020**, *32* (22), 1–6.
- (31) Bardeen, C. J. The Structure and Dynamics of Molecular Excitons. *Annu. Rev. Phys. Chem.* **2014**, *65* (1), 127–148.
- (32) Ompong, D.; Singh, J. Diffusion Length and Langevin Recombination of Singlet and Triplet Excitons in Organic Heterojunction Solar Cells. *ChemPhysChem* **2015**, *16* (6), 1281–1285.
- (33) Tamai, Y.; Ohkita, H.; Bente, H.; Ito, S. Exciton Diffusion in Conjugated Polymers: From Fundamental Understanding to Improvement in Photovoltaic Conversion Efficiency. *J. Phys. Chem. Lett.* **2015**, *6* (17), 3417–3428.

- (34) Jin, Y.; Zhang, Y.; Liu, Y.; Xue, J.; Li, W.; Qiao, J.; Zhang, F. Limitations and Perspectives on Triplet-Material-Based Organic Photovoltaic Devices. *Adv. Mater.* **2019**, *31* (22), 1–18.
- (35) Qin, L.; Liu, X.; Zhang, X.; Yu, J.; Yang, L.; Zhao, F.; Huang, M.; Wang, K.; Wu, X.; Li, Y.; et al. Triplet Acceptors with a D-A Structure and Twisted Conformation for Efficient Organic Solar Cells. *Angew. Chemie - Int. Ed.* **2020**, *59* (35), 15043–15049.
- (36) Hummer, K.; Ambrosch-Draxl, C. Oligoacene Exciton Binding Energies: Their Dependence on Molecular Size. *Phys. Rev. B - Condens. Matter Mater. Phys.* **2005**, *71* (8), 1–4.
- (37) Hu, Z.; Zhou, B.; Sun, Z.; Sun, H. Prediction of Excited-State Properties of Oligoacene Crystals Using Polarizable Continuum Model-Tuned Range-Separated Hybrid Functional Approach. *J. Comput. Chem.* **2017**, *38* (9), 569–575.
- (38) Chen, X. K.; Kim, D.; Brédas, J. L. Thermally Activated Delayed Fluorescence (TADF) Path toward Efficient Electroluminescence in Purely Organic Materials: Molecular Level Insight. *Acc. Chem. Res.* **2018**, *51* (9), 2215–2224.
- (39) Tanaka, H.; Shizu, K.; Miyazaki, H.; Adachi, C. Efficient Green Thermally Activated Delayed Fluorescence (TADF) from a Phenoxazine–Triphenyltriazine (PXZ–TRZ) Derivative. *Chem. Commun.* **2012**, *48* (93), 11392–11394.
- (40) Yuan, J.; Zhang, Y.; Zhou, L.; Zhang, G.; Yip, H. L.; Lau, T. K.; Lu, X.; Zhu, C.; Peng, H.; Johnson, P. A.; et al. Single-Junction Organic Solar Cell with over 15% Efficiency Using Fused-Ring Acceptor with Electron-Deficient Core. *Joule* **2019**, *3* (4), 1140–1151.
- (41) Zhu, X.; Zhang, G.; Zhang, J.; Yip, H. L.; Hu, B. Self-Stimulated Dissociation in Non-Fullerene Organic Bulk-Heterojunction Solar Cells. *Joule* **2020**, *4* (11), 2443–2457.
- (42) Wang, T.; Brédas, J. Quantum-Chemical Evaluation of Impact of Chlorination versus Fluorination on the Electronic Properties of Donors and Acceptors for Organic Solar Cells. *Adv. Theory Simulations* **2019**, 1900136.
- (43) Qu, J.; Chen, H.; Zhou, J.; Lai, H.; Liu, T.; Chao, P.; Li, D.; Xie, Z.; He, F.; Ma, Y. Chlorine Atom-Induced Molecular Interlocked Network in a Non-Fullerene Acceptor. *ACS Appl. Mater. Interfaces* **2018**, *10* (46), 39992–40000.
- (44) Zhang, H.; Yao, H.; Hou, J.; Zhu, J.; Zhang, J.; Li, W.; Yu, R.; Gao, B.; Zhang, S.; Hou, J. Over 14% Efficiency in Organic Solar Cells Enabled by Chlorinated Nonfullerene Small-Molecule Acceptors. *Adv. Mater.* **2018**, *30* (28), 1–7.

- (45) Zhang, Y.; Yao, H.; Zhang, S.; Qin, Y.; Zhang, J.; Yang, L.; Li, W.; Wei, Z.; Gao, F.; Hou, J. Fluorination vs. Chlorination: A Case Study on High Performance Organic Photovoltaic Materials. *Sci. China Chem.* **2018**, *61* (10), 1328–1337.
- (46) Geng, R.; Song, X.; Feng, H.; Yu, J.; Zhang, M.; Gasparini, N.; Zhang, Z.; Liu, F.; Baran, D.; Tang, W. Nonfullerene Acceptor for Organic Solar Cells with Chlorination on Dithieno[3,2- b:2',3'- d]Pyrrol Fused-Ring. *ACS Energy Lett.* **2019**, *4* (3), 763–770.
- (47) Li, S.; Ye, L.; Zhao, W.; Zhang, S.; Mukherjee, S.; Ade, H.; Hou, J. Energy-Level Modulation of Small-Molecule Electron Acceptors to Achieve over 12% Efficiency in Polymer Solar Cells. *Adv. Mater.* **2016**, *28* (42), 9423–9429.
- (48) Fan, B.; Du, X.; Liu, F.; Zhong, W.; Ying, L.; Xie, R.; Tang, X.; An, K.; Xin, J.; Li, N.; et al. Fine-Tuning of the Chemical Structure of Photoactive Materials for Highly Efficient Organic Photovoltaics. *Nat. Energy* **2018**, *3* (12), 1051–1058.
- (49) Zhao, W.; Qian, D.; Zhang, S.; Li, S.; Inganäs, O.; Gao, F.; Hou, J. Fullerene-Free Polymer Solar Cells with over 11% Efficiency and Excellent Thermal Stability. *Adv. Mater.* **2016**, 4734–4739.
- (50) Zhao, W.; Li, S.; Yao, H.; Zhang, S.; Zhang, Y.; Yang, B.; Hou, J. Molecular Optimization Enables over 13% Efficiency in Organic Solar Cells. *J. Am. Chem. Soc.* **2017**, *139* (21), 7148–7151.
- (51) Yao, H.; Chen, Y.; Qin, Y.; Yu, R.; Cui, Y.; Yang, B.; Li, S.; Zhang, K.; Hou, J. Design and Synthesis of a Low Bandgap Small Molecule Acceptor for Efficient Polymer Solar Cells. *Adv. Mater.* **2016**, *28* (37), 8283–8287.
- (52) Yao, H.; Cui, Y.; Yu, R.; Gao, B.; Zhang, H.; Hou, J. Design, Synthesis, and Photovoltaic Characterization of a Small Molecular Acceptor with an Ultra-Narrow Band Gap. *Angew. Chemie - Int. Ed.* **2017**, *56* (11), 3045–3049.
- (53) Cui, Y.; Yang, C.; Yao, H.; Zhu, J.; Wang, Y.; Jia, G.; Gao, F.; Hou, J. Efficient Semitransparent Organic Solar Cells with Tunable Color Enabled by an Ultralow-Bandgap Nonfullerene Acceptor. *Adv. Mater.* **2017**, *29* (43), 1–7.
- (54) Frisch, M. J.; Trucks, G. W.; Schlegel, H. B.; Scuseria, G. E.; Robb, M. A.; Cheeseman, J. R.; Scalmani, G.; Barone, V.; Mennucci, B.; Petersson, G. A.; et al. Gaussian 16, Revision C.01. *Gaussian, Inc., Wallingford CT* **2016**.
- (55) Becke, A. D. Density-Functional Thermochemistry. III. The Role of Exact Exchange. *J. Chem. Phys.* **1993**, *98* (7), 5648–5652.
- (56) Chai, J.-D.; Head-Gordon, M. Long-Range Corrected Hybrid Density Functionals with Damped Atom–Atom Dispersion Corrections. *Phys. Chem. Chem. Phys.* **2008**, *10* (44), 6615–6620.

- (57) Zheng, Z.; Brédas, J.-L.; Coropceanu, V. Description of the Charge Transfer States at the Pentacene/C60 Interface: Combining Range-Separated Hybrid Functionals with the Polarizable Continuum Model. *J. Phys. Chem. Lett.* **2016**, *7* (13), 2616–2621.
- (58) Stein, T.; Kronik, L.; Baer, R. Reliable Prediction of Charge Transfer Excitations in Molecular Complexes using Time-Dependent Density Functional Theory. *J. Am. Chem. Soc.* **2009**, *131* (8), 2818–2820.
- (59) Tumbleston, J. R.; Collins, B. A.; Yang, L.; Stuart, A. C.; Gann, E.; Ma, W.; You, W.; Ade, H. The Influence of Molecular Orientation on Organic Bulk Heterojunction Solar Cells. *Nat. Photonics* **2014**, *8* (5), 385–391.
- (60) Bredas, J.-L. Mind the Gap! *Mater. Horiz.* **2014**, *1* (1), 17–19.
- (61) Barone, V.; Cossi, M.; Tomasi, J. A New Definition of Cavities for the Computation of Solvation Free Energies by the Polarizable Continuum Model. *J. Chem. Phys.* **1997**, *107* (8), 3210–3221.
- (62) Sun, H.; Hu, Z.; Zhong, C.; Zhang, S.; Sun, Z. Quantitative Estimation of Exciton Binding Energy of Polythiophene-Derived Polymers Using Polarizable Continuum Model Tuned Range-Separated Density Functional. *J. Phys. Chem. C* **2016**, *120* (15), 8048–8055.
- (63) Benatto, L.; Koehler, M. Effects of Fluorination on Exciton Binding Energy and Charge Transport of π -Conjugated Donor Polymers and the ITIC Molecular Acceptor: A Theoretical Study. *J. Phys. Chem. C* **2019**, *123* (11), 6395–6406.
- (64) Benatto, L.; Moraes, C. A. M.; Candiotto, G.; Sousa, K. R. A.; Souza, J. P. A.; Roman, L. S.; Koehler, M. Conditions for Efficient Charge Generation Preceded by Energy Transfer Process in Non-Fullerene Organic Solar Cells. *J. Mater. Chem. A* **2021**, Advance Article.
- (65) Cox, S. R.; Williams, D. E. Representation of the Molecular Electrostatic Potential by a Net Atomic Charge Model. *J. Comput. Chem.* **1981**, *2* (3), 304–323.
- (66) Singh, U. C.; Kollman, P. A. An Approach to Computing Electrostatic Charges for Molecules. *J. Comput. Chem.* **1984**, *5* (2), 129–145.
- (67) Londi, G.; Dilmurat, R.; D’Avino, G.; Lemaury, V.; Olivier, Y.; Beljonne, D. Comprehensive Modelling Study of Singlet Exciton Diffusion in Donor-Acceptor Dyads: When Small Changes in Chemical Structure Matter. *Phys. Chem. Chem. Phys.* **2019**, *21* (45), 25023–25034.
- (68) Lu, T.; Chen, F. Multiwfn: A Multifunctional Wavefunction Analyzer. *J. Comput. Chem.* **2012**, *33* (5), 580–592.

- (69) Yang, C.; Zhang, J.; Liang, N.; Yao, H.; Wei, Z.; He, C.; Yuan, X.; Hou, J. Effects of Energy-Level Offset between a Donor and Acceptor on the Photovoltaic Performance of Non-Fullerene Organic Solar Cells. *J. Mater. Chem. A* **2019**, *7* (32), 18889–18897.
- (70) Zhang, D. Di; Yang, X.; Zheng, X.; Yang, W. Accurate Density Functional Prediction of Molecular Electron Affinity with the Scaling Corrected Kohn–Sham Frontier Orbital Energies. *Mol. Phys.* **2018**, *116* (7–8), 927–934.
- (71) Zhang, S.; Qin, Y.; Zhu, J.; Hou, J. Over 14% Efficiency in Polymer Solar Cells Enabled by a Chlorinated Polymer Donor. *Adv. Mater.* **2018**, *30* (20), 1–7.
- (72) Ming, L. T.; Joon, H. O.; Reichardt, A. D.; Bao, Z. Chlorination: A General Route toward Electron Transport in Organic Semiconductors. *J. Am. Chem. Soc.* **2009**, *131* (10), 3733–3740.
- (73) Liu, X.; Li, Y.; Ding, K.; Forrest, S. Energy Loss in Organic Photovoltaics: Nonfullerene Versus Fullerene Acceptors. *Phys. Rev. Appl.* **2019**, *11* (2), 024060.
- (74) Yang, L.; Qin, L.; Xu, Y.; Zhang, H.; Lv, L.; Chen, K.; Sui, X.; Zhong, Y.; Guo, Y.; Gao, F.; et al. Sulfur vs. Tellurium: The Heteroatom Effects on the Nonfullerene Acceptors. *Sci. China Chem.* **2019**, *62* (7), 897–903.
- (75) Chen, Z.; Chen, X.; Jia, Z.; Zhou, G.; Xu, J.; Wu, Y.; Xia, X.; Li, X.; Zhang, X.; Deng, C.; et al. Triplet Exciton Formation for Non-Radiative Voltage Loss in High-Efficiency Nonfullerene Organic Solar Cells. *Joule* **2021**, *5* (7), 1832–1844.
- (76) Benatto, L.; Sousa, K. R. A.; Koehler, M. Driving Force for Exciton Dissociation in Organic Solar Cells: The Influence of Donor and Acceptor Relative Orientation. *J. Phys. Chem. C* **2020**, *124* (25), 13580–13591.
- (77) Zhu, L.; Tu, Z.; Yi, Y.; Wei, Z. Achieving Small Exciton Binding Energies in Small Molecule Acceptors for Organic Solar Cells: Effect of Molecular Packing. *J. Phys. Chem. Lett.* **2019**, *10* (17), 4888–4894.
- (78) Aizawa, N.; Harabuchi, Y.; Maeda, S.; Pu, Y. J. Kinetic Prediction of Reverse Intersystem Crossing in Organic Donor–Acceptor Molecules. *Nat. Commun.* **2020**, *11* (1), 1–6.
- (79) Chow, P. C. Y.; Chan, C. C. S.; Ma, C.; Zou, X.; Yan, H.; Wong, K. S. Factors That Prevent Spin-Triplet Recombination in Non-Fullerene Organic Photovoltaics. *J. Phys. Chem. Lett.* **2021**, *12*, 5045–5051.
- (80) Williams, R. M.; Chen, H. C.; Di Nuzzo, D.; Meskers, S. C. J.; Janssen, R. A. J. Ultrafast Charge and Triplet State Formation in Diketopyrrolopyrrole Low Band Gap Polymer/Fullerene Blends: Influence of Nanoscale Morphology of Organic Photovoltaic Materials on Charge Recombination to the Triplet State. *J.*

Spectrosc. **2017**, *2017*.

- (81) Wang, Z.; Liu, H.; Xie, X.; Zhang, C.; Wang, R.; Chen, L.; Xu, Y.; Ma, H.; Fang, W.; Yao, Y.; et al. Free-Triplet Generation with Improved Efficiency in Tetracene Oligomers through Spatially Separated Triplet Pair States. *Nat. Chem.* **2021**, *13*, 559–567.
- (82) Natsuda, S. I.; Sakamoto, Y.; Takeyama, T.; Shirouchi, R.; Saito, T.; Tamai, Y.; Ohkita, H. Singlet and Triplet Excited-State Dynamics of a Nonfullerene Electron Acceptor Y6. *J. Phys. Chem. C* **2021**, *125* (38), 20806–20813.
- (83) Zhao, Q.; Qu, J.; He, F. Chlorination: An Effective Strategy for High-Performance Organic Solar Cells. *Adv. Sci.* **2020**, *7* (14), 1–25.